How do the fluid dynamics change for gravity-destabilized film flow on structured surfaces? An experimental investigation using light-induced fluorescence*

Hannes Raddant[a,*], Georg Brösigke[a], Christian Hoffmann[a], Markus Illner[a], Jens-Uwe Repke[a]

[a] *Technische Universität Berlin, Process Dynamics and Operations Group, Sekr. KWT 9, Straße des 17. Juni 135, 10623 Berlin, Germany*

Abstract

Liquid film flow is the dominant flow regime in distillation and absorption processes within structured packings. Extensive research has been carried out to improve the understanding of the involved fluid dynamics. Up to now, these investigations mainly focused on gravity-stabilized film flow, i.e., the liquid phase flows over a packing in counter-current flow with a gas phase. In contrast, gravity-destabilized film flow is studied much less frequently al-

*This is the Accepted Manuscript of: Raddant, H., Brösigke, G., Hoffmann, C., Illner, M., Repke, J.-U. (2023). How do the fluid dynamics change for gravity-destabilized film flow on structured surfaces? An experimental investigation using light-induced fluorescence. Chemical Engineering Research and Design, Vol. 196, pp. 390-403.
https://doi.org/10.1016/j.cherd.2023.06.052.

*Corresponding authors

Email addresses: raddant@tu-berlin.de (Hannes Raddant), georg.broesigke@tu-berlin.de (Georg Brösigke), c.hoffmann@tu-berlin.de (Christian Hoffmann), markus.illner@tu-berlin.de (Markus Illner), j.repke@tu-berlin.de (Jens-Uwe Repke)

though this type of flow applies to about half of the cases in a column with structured packings. Here, the liquid runs along the underside of the packing, also in counter-current flow with the gas phase. To close the gap in the experimental data, this contribution investigates the fundamental fluid dynamics of gravity-destabilized liquid film flows on a smooth plate, a 2D wave texture, and a 3D pyramidal texture. Results on critical convective inclination angle, drained liquid mass flow, and liquid film thickness without gas counter-current gas flow are reported and compared to numerical results from literature. In the experiments, the Reynolds number is varied from 28.4 to 113.5 using a surfactant-modified aqueous system. The 2D structure showed decreased liquid flow stability compared to the smooth surface. However, the 3D structure seems to have a stabilizing effect on the flow.
Keywords: Fluid dynamics, Film flow, Structured surface, Rayleigh-Taylor instability, Negative inclination angle

Nomenclature

Abbreviations

CCD	Charged-coupled device
CFD	Computational fluid dynamics
LIF	Light-induced Fluorescence
RTI	Rayleigh-Taylor instabilities
ROI	Region of interest
WRIBL	Weighed residual integral boundary layer
2D	Two-dimensional
3D	Three-dimensional

Dimensionless numbers

Ka	Kapitza number
Re	Reynolds number

Greek Symbols

α	Inclination angle in °
α^*	Experimental critical convective inclination angle in °
β	Inclination angle in °
δ	Liquid film thickness in mm
δ^*	Liquid film thickness normalized to structure height in $-$
λ	Wavelength in nm
ρ	Density in $\mathrm{kg\,m^{-3}}$
μ	Kinematic viscosity in $\mathrm{m^2\,s^{-1}}$
σ	Surface tension in $\mathrm{N\,m^{-1}}$
θ	Inclination angle in ° (same orientation as α)

Latin Symbols

c	Concentration in $\mathrm{mg\,L^{-1}}$
m	Share of drained liquid mass flow in %

w	Width in m
q	Specific volume flow in $m^2\,s^{-1}$
V	Volume flow in $m^3\,s^{-1}$

Indices

c	Index for component, $c \in 1 \ldots N_c$

Subscripts

abs	Absorption
c	Capillary
calc	Calculated
cmc	Critical micellar concentration
crit	Critical
em	Emission
ex	Excitation
exp	Experimental
l	Liquid
mean	Mean value
rel	Relative
sim	Simulative

1. Introduction

Over the past decades, structured packings have been intensively studied (Spiegel and Duss, 2014) and used in distillation (Billingham and Lockett, 1999; Kiss, 2019) and absorption processes (Aroonwilas, 2001; Flagiello et al., 2019). A major research focus has been the impact of structured surfaces of packing materials on fluid dynamics, e.g., in terms of pressure drop and separation performance.

Film and rivulet flow are the dominating flow regimes in the liquid phase on a structured surface material (Green et al., 2007; Aferka et al., 2011; Repke et al., 2011; Janzen et al., 2013). The liquid flow over the packing structure is mainly present as a film flow (Aferka et al., 2011; Repke et al., 2011) and rivulet flow occurs primarily among contiguous packing materials (Janzen et al., 2013). For overflowed plates, used as approximation for packing material, the flow changes with different inclinations and both flow regimes can occur as found by Charogiannis et al. (2018). Besides distillation and absorption processes, film flows are also present in various other applications, e.g., heat exchangers, evaporators and condensators (Abdelall et al., 2006; Kalliadasis et al., 2011). Due to its appearance in so many applications, a fundamental understanding of film flow is highly desired to accurately design and model structured packings or even whole columns.

In general, the fluid dynamic behavior of film flows is based on a complex balance of forces which permanently aims at minimizing the liquid surface. Hence, different flow regimes are expected, e.g., wavy film flows (Alekseenko et al., 1994). Moreover, thermal and morphologic effects influence the fluid dynamic behavior of a film flow (Kapitza and Kapitza, 1949; Kalliadasis

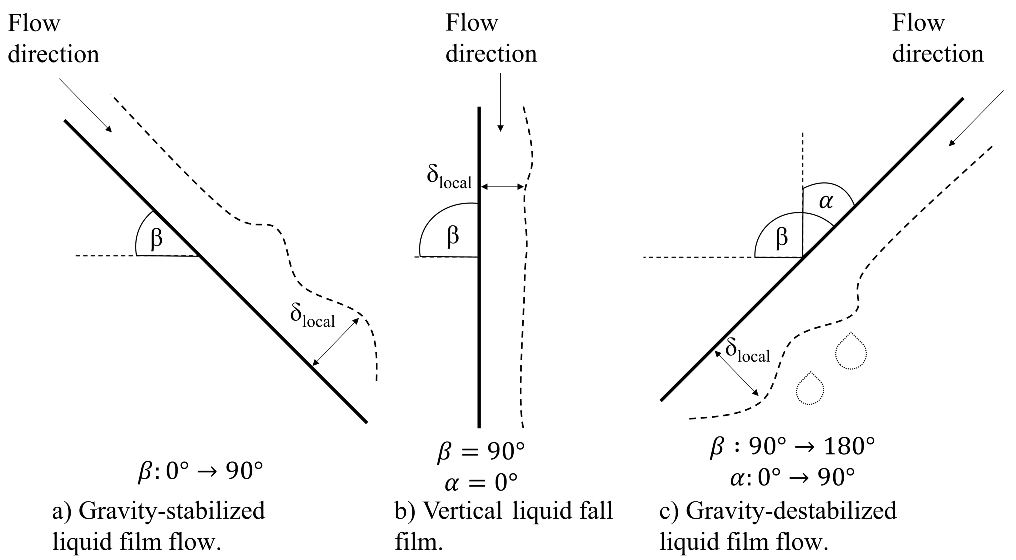

Figure 1: Possible regimes regarding the liquid flow on a solid surface for different inclination angles: a) $0^\circ \leq \beta < 90^\circ$, b) $\beta = 90^\circ$ and $\alpha = 0^\circ$, c) $90^\circ < \beta \leq 180^\circ$ and $0^\circ < \alpha \leq 90^\circ$.

et al., 2011). There are three different cases for the range of conceivable inclination angles (Rohlfs et al., 2017):

(a) the gravity-stabilized case;

(b) the vertical case;

(c) the gravity-destabilized case.

These cases are visualized in Figure 1. In case a), the liquid flows on top of a solid surface with an overlying gas phase. The gravity stabilizes the flow and Rayleigh-Taylor instabilities can not occur (Rietz et al., 2017). Case b) represents a vertical fall film, which is of minor relevance for the flow regime in structured packings due to the corrugated morphology and not further discussed. In case c), a liquid phase flows along the bottom of a solid surface with an underlying gas phase. For this reason the less dense gas phase flows under the more dense liquid phase causing a density difference in the direction of gravity. As a consequence due to induced interaction of the liquid phase with the gas phase Rayleigh-Taylor instabilities could be evolved (Chandrasekhar, 1961; Sharp, 1984).

In the next section, we present a brief literature review of experimental and numerical investigations on gravity-stabilized and gravity-destabilized flow. Based on this review, we show that there is insufficient experimental data for gravity-destabilized flow on structured surfaces below and above the critical inclination angle and at various operating conditions as quantified by the dimensionless Reynolds and Kapitza numbers. Afterwards, Section 3 introduces the measurement cell that was constructed to conduct the experiments. Finally, Section 4 presents the results and contains a thorough discussion of the obtained data, including the comparison with numerically determined values by other authors. The contribution concludes with a brief summary and an outlook to future research.

2. Literature review and theoretical background

The following section extends the theoretical background regarding gravity-stabilized film flow in Section 2.1 and for gravity-destabilized film flow in Section 2.2. In favor the decisive fluid dynamics and there differences as well as the influence of surface structures are explained.

2.1. Gravity-stabilized film flow

Gravity-stabilized film flows have been studied extensively, both experimentally and numerically. For the gravity-stabilized film flow, several flow regimes may occur depending on the Reynolds number, i.e., laminar (Re $\leq$ 5.7), stable wave (25 $\leq$ Re $\leq$ 75), turbulent flow (Re $\geq$ 400) as well as two transitions flow regimes between these Reynolds numbers (Ishigai et al., 1972).

The Reynolds number is defined as written in Equation (1). In this equation, q_{l} is the volume flow related to the plate width w_{surface} and μ_{l} is the kinematic viscosity of the liquid phase.

$$\mathrm{Re} = \frac{q_{\mathrm{l}}}{\mu_{\mathrm{l}}} \text{ with } q_{\mathrm{l}} = \frac{V_{\mathrm{l}}}{w_{\mathrm{surface}}}, \tag{1}$$

For a smooth surface, the force balance for a laminar film flow can be described by the Nusselt correlation (Nusselt, 1916). Equation (2) is based on the Reynolds number Re, the inclination angle α, and the kinematic viscosity of the liquid phase μ_{l} and is valid up to Reynolds number of 400 (Brauer, 1956; Scheid et al., 2016).

$$\delta = \left(\frac{3 \cdot \mu_l^2}{g \cdot \cos\alpha} \right)^{\frac{1}{3}} \cdot Re^{\frac{1}{3}} \tag{2}$$

Its solution describes the liquid film thickness depending on property data (e.g., viscosity μ_{l}), the Reynolds number Re, and gravitational acceleration for a smooth $g \cdot \cos\alpha$ laminar film flow. The Nusselt correlation was validated on a smooth surface using different measurement methods (Brauer, 1971; Lel et al., 2005). A theoretical investigation of different film flow regimes and characteristic wave patterns was presented by Alekseenko et al. (1994). Furthermore, semi-empirical equations for the film thickness and velocity for occurring stable waves in gravity-stabilized film flows were reported by Brauer (1971) and Al-Sibai (2004).

For the more generic case of plates with microstructure, Zhao and Cerro (1992) demonstrated the influence of the ratio between the liquid film thickness and microstructure height (δ^*) on the fluid dynamics. They differed between the following regimes:

Regime 1: $\delta^* < 0.1$; the liquid flow follows the contour of the structured surface.

Regime 2: $0.1 < \delta^* < 1$; the fluid dynamics of the liquid film are highly influenced by the structured surface and specific liquid flow phenomena are expected.

Regime 3: $\delta^* > 1$; The film thickness is noticeably higher than the structure resulting in a minor structure influence on the liquid flow.

Over the last 20 years, technological improvements in computer science and laser technology have allowed a temporally and locally resolved analysis of gravity-stabilized film flows (Al-Sibai, 2004; Lel et al., 2005). Furthermore, film flows over structured surfaces of various types were investigated intensively, e.g., for different micro- and macrostructured surfaces (Zhao and Cerro, 1992), and for an inclined wall with sinussoidal corrugations (Bontozoglou and Papapolymerou, 1997). Moreover, film flows over an inclined periodic wall with rectangular corrugations were investigated by Vlachogiannis and Bontozoglou (2002). To study the effect of corrugation steepness, film flows for inclination angle from 1° up to 15° and Reynolds numbers from 10 up to 450 over an inclined periodic wall with transverse rectangular corrugations were investigated by Argyriadi et al. (2006) and found a stabilization effect on the critical Reynolds number with increased corrugation steepness.

Moreover, one-phase and two-phase film flows over tetrahedron and lamellar structures were studied by Paschke (2011). The liquid film thickness and liquid holdup on a real packing for different liquid loads was investigated by Leuner et al. (2018b) using two different measurement cell designs and a successful comparison with literature correlations was shown. Likewise, the local velocity and film thickness on corrugated structured packing geometries were presented by Gerke et al. (2018) and found an increased mixing across the liquid film, although similar orders for the velocity distribution over the film thickness were found experimentally.

In addition to the experimental work, numerical investigations and modeling of the fluid dynamics of film flows over structured surfaces were carried out. For a wave structure, modeling and validation by experiments was reported by Shetty and Cerro (1993). Szulczewska et al. (2003) performed simulations of liquid flows over packing structures using computation fluid dynamics (CFD) and validated their simulations with experiments. In addition, Trifonov (2011) studied the fluid dynamics of film flows on vertical corrugated plates numerically and experimentally. The influence of a single microstructure, with variations in height and form, on vortex formation and the interfacial area on the lying film flow was numerically investigated by Bonart and Repke (2018). The authors found no effect of microstructures with small heights compared to the film thickness on the enhancement of the interfacial area, however large structures could increase the interfacial area.

As evident from this review, there is a vast body of literature on experimental and numerical investigations for gravity-stabilized film flows for various geometries and operating conditions. Consequentially, we excluded this flow regime from our investigations within this contribution.

2.2. Gravity-destabilized film flow

In contrast to gravity-stabilized film flows, the understanding of fluid dynamics of gravity-destabilized film flows is limited. Only in the last decade, significant contributions in this area have been reported. The liquid phase flows along the bottom of the packing material and on top of a gas phase as shown in Figure 2. For this reason the less dense gas phase flows under the more dense liquid phase causing a density difference in the direction of gravity. Two forms of instabilities are possible as shown in Figure 2: the convective Rayleigh-Taylor instability (case a)) and the absolute Rayleigh-Taylor instability (case b)). The former is characterized by a predominant effect of the surface tension on the overall liquid film stability or an inertia dominated region as described by Scheid et al. (2016). For lower Reynolds numbers the surface tension stabilizes the film flow because the flow velocity is relatively low. For higher Reynolds numbers, inertia dominates the flow stability. The convective Rayleigh-Taylor instability is characterized by more dominant convective transport of perturbations compared to the local growth rate of instabilities, amplification, or damping with increasing run time respectively length (Brun et al., 2015). The disturbance can occur at small run lengths and is transported away from its origin due to the convective flow. For the latter, gravity dominates the surface tension and inertia stabilization mechanism so that continuous and regular droplet detachment from the liquid flow at a spatial fixed position occurs. Therefore, the absolute Rayleigh-Taylor instabilty is present when perturbations grow exponentially regardless of an existing convective flow, resulting in a spatially fixed position

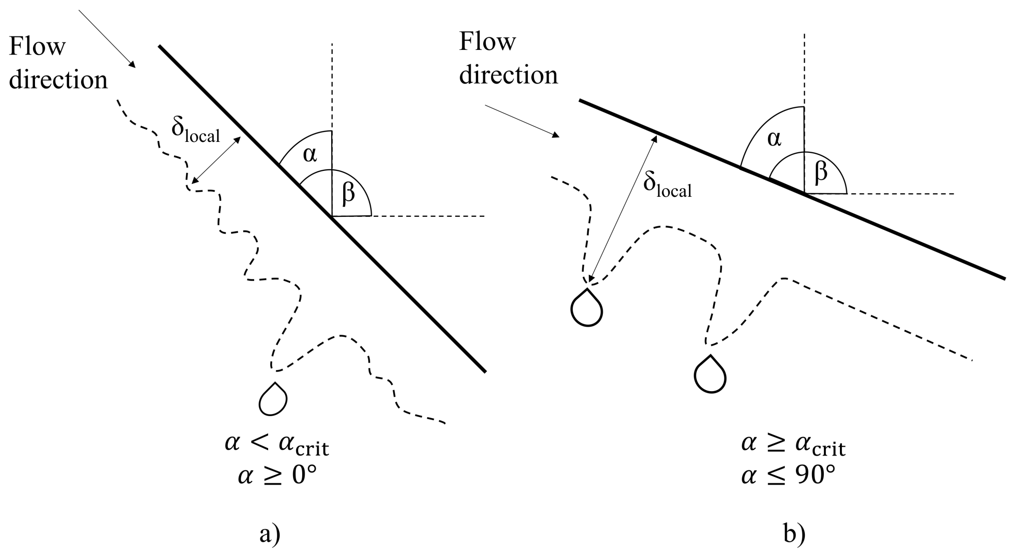

Figure 2: Possible sub-cases of gravity-destabilized liquid flow flow: a) - convective Rayleigh-Taylor instability, $\alpha < \alpha_{\mathrm{crit}}$; b) - absolute Rayleigh-Taylor instability, $\alpha \geq \alpha_{\mathrm{crit}}$.

of the perturbation and in a propagation speed of the perturbation of zero Brun et al. (2015). Overall, the critical inclination angle marks the transition between convective and absolute Rayleigh-Taylor instability.

According to Brun et al. (2015), the capillary length is defined as

$$l_{\mathrm{c}} = \sqrt{\frac{\sigma_{\mathrm{l}}}{\rho_{\mathrm{l}} g}}, \tag{3}$$

based on the liquid surface tension σ_{l}, the liquid density ρ_{l} and the gravity constant g. First experiments to determine the critical inclination angle on smooth surfaces for a laminar film flow performed by Brun et al. (2015) demonstrated a significant influence of the ratio between the liquid film thickness and the capillary length. An increase of the aforementioned ratio leads to a smaller critical angle, as reported by (Brun et al., 2015). At this point, we present the definition of the Kapitza number, as it is the second important dimensionless number for the entire article.

Equation (4) shows the definition of the Kapitza number (Scheid et al., 2016; Kofman et al., 2017).

$$\mathrm{Ka} = \frac{\sigma_{\mathrm{l}}}{g^{\frac{1}{3}} \cdot \mu_{\mathrm{l}}^{\frac{4}{3}} \cdot \rho_l}. \tag{4}$$

The definition of the Kapitza number for the vertical case as in Kofman et al. (2017) is used for the contribution. The numerical simulations of Scheid et al. (2016) showed that the occurrence of Rayleigh-Taylor instabilities depends on the Reynolds number, the Kapitza number, and the inclination angle α at least for film flow over a smooth surface. An influence of the microstructure on the liquid flow was not investigated. Scheid et al. (2016) developed their model based on the lubrication method to determine the linear transition between absolute and convective Rayleigh-Taylor instability designated as the critical inclination angle numerically. They extended this model by inertial forces and made it applicable to higher Reynolds numbers up to 60. The minimal critical inclination angle on a smooth surface for Kapitza numbers from 2^{-3} to 1^{11} was investigated by Scheid et al. (2016). For smaller angles than the minimal critical angle of 57.4°, absolute Rayleigh-Taylor instability is not present. However, it was concluded that the critical inclination angle depends on the Reynolds number and the Kapitza number overall. Therefore, convective instability is dominated by two mechanisms: the surface tension dominates the stabilization of the film flow until a minimum of the critical inclination angle for increasing Reynolds number is reached. After exceeding this minimal angle, an inertia-dominated convective instability region is reached. Both stabilization mechanisms lead to larger critical inclination angles for a constant Kapitza number. Regardless of the stabilization mechanism, gravity induces instabilities in both regions. The flow is stabilized with rising Reynolds number, which leads to higher critical inclination angles for the region above the minimum critical angle reported by Scheid et al. (2016). The film flow is convective unstable, even if Scheid et al. (2016) found an increasing critical inclination angle for increasing Reynolds number after exceeding the minimal critical angle. Additional direct numerical simulations and another methodology (WRIBL) was applied on the modelling of gravity-destabilized film flows for different wave types e.g. solitary-like waves and sinussoidal-like waves and showed eddy formations in wave crests (Rohlfs and Scheid, 2015; Rohlfs et al., 2017). These eddy formations are promoted by structured surfaces and can be suppressed by adding surfactants (Davies, 1972).

Besides the work of Scheid et al. (2016), Kofman et al. (2017) carried out numerical simulations with the Navier-Stokes equation as well as with another modelling approach (WRIBL) of gravity-destabilized film flow over smooth surfaces regarding the two-dimensional dripping onset. Kofman et al. (2017) concluded, that the linear absolute to convective instability transition is insufficiently predicting the dripping limit and highlight the importance of non-linear effects. Experimental investigations on a rotating cylinder as well as numerical studies are carried out by Rietz et al. (2017) and a major influence of the flow condition on droplet detachment induced by wave or rivulet coalescence was observed. Rietz et al. (2017) concluded the transition of the film instability mechanism from Kapitza instability to Rayleigh-Taylor instability is unclear and could be a sharp or a continuous conversion.

The number of experimental studies on gravity-destabilized film flows is very limited. Besides the work of Brun et al. (2015), Alekseenko et al. (2007) observed the velocity field of a gravity-destabilized film flow around a circular cylinder. Charogiannis et al. (2018) investigated gravity-destabilized film flow on flat soda lime glass plate for inclination angles between $-15°$ and $-45°$ for two Kapitza numbers as well as Reynolds numbers between 0.6 and 193. They found no droplet detachment in the investigated range of inclination angles and reported data for liquid film thickness and wavelength for film and rivulets flow. Lerisson et al. (2020) studied steady flow patterns of film flow on a glass plate for inclination angles θ in the range of 20° to 60°, reported the thickness of the liquid film, and carried out a stability analysis. They found cases where rivulets could suppress or significantly increase liquid dripping effects. Finally, Ledda et al. (2020, 2021) also performed a stability analysis and measurements of the film thickness on a smooth surface for θ in the range from 20° up to 80°. For a forced steady flow, spanwise parallel rivulets were found. They also discuss a possible destabilizing effect with increasing flow length caused by traveling lenses on top of the rivulets. Rietz et al. (2021) investigated numerically the formation of rivulets and the wavelength in the case of Rayleigh-Taylor instability for inclination angles α between 0° to 75°. They observed parallel rivulet flow with increasing inclination angle and compared two scenarios ($\mathrm{Re} = 1$, $\mathrm{Ka}_{\alpha=0^\circ} = 13.1$ and $\mathrm{Re} = 40$, $\mathrm{Ka}_{\alpha=0^\circ} = 330$) to the work of Charogiannis et al. (2018).

So far, the experimental investigations found in the literature studied exclusively gravity-destabilized film flows on smooth surfaces and no experimental investigations on structured surfaces were carried out. In addition, only Ledda et al. (2020) investigated experimentally film flows for $\alpha > \alpha_{\mathrm{crit}}$.

Beside that, no experiments for inclination angles α up to 90° were reported. To fill this gap, we present new experimental data for the full range of inclination angles between 0° and 90° for a wide range of Reynolds numbers (28.4 to 113.5). Next to the critical inclination angle α_{crit}, the relative drained liquid mass flow $m_{\mathrm{rel,exp}}$ (i.e., the ratio of drained liquid to feed) is determined as a function of the inclination angle α and the Reynolds number. For inclination angles above the critical one α_{crit}, liquid drains off the surface in a not yet known amount. A quantification of the drained liquid flow $m_{\mathrm{rel,exp}}$ and the mean liquid film thickness δ_{mean} is determined as a function of the inclination angle α and the Reynolds number as well as the surface structure. The experiments are carried out for a smooth surface, a 2D wave structure, and a 3D pyramidal structure. These structures were designed so that δ^* lies between 0.1 and 1.0 as reported by Zhao and Cerro (1992). Finally, we compare our results with the numerically determined critical inclination angles on a smooth surface for the linear absolute/convective transition published by Scheid et al. (2016).

In Figure 2, two possible flow conditions for gravity-destabilized film flows are shown. The case a) represents the transition state of gravity-destabilized film flow for $\alpha < \alpha_{\mathrm{crit}}$. Here, convective Rayleigh-Taylor instabilities can occur solely until α_{crit} is reached (Scheid et al., 2016). The gravity induced acceleration of the liquid decreases with increasing α and a higher influence of the surface tension or inertia on the formation of the flow is pronounced. Hence, changes in the flow regime from film flow regime for $\alpha = 0°$ to parallel rivulet flow regime for increasing α appear to be found experimentally (Charogiannis et al., 2018) and numerically (Rietz et al., 2021). As a result, different liquid flow regimes are present: 1) film flow, 2) ripped film flow and 3) rivulet flow which occur simultaneously. The mean liquid film thickness δ_{mean} rises due to less acceleration of the liquid film in case a) in Figure 2. Due to additional inertial forces, the Nusselt's solution for laminar film flow is no longer fulfilled (Zhao and Cerro, 1992; Vlachogiannis and Bontozoglou, 2002). Nevertheless, the liquid film thickness δ for smooth and wavy laminar film flow can still be calculated with acceptable accuracy using Equation (2), but definitly for the vertical film flow. Likewise, the Reynolds number and the surface structure should have a significant influence on the mean film thickness δ_{mean}. An increased ripple of the flow and a higher tendency of droplet formation is observed for increasing inclination angle and for higher Reynolds number (Kofman et al., 2017). For the case of convective Rayleigh-Taylor instabilities wave merging can occur (Kofman et al., 2017) and near α_{crit} random and irregular liquid detachment out of the flow may appear. The critical inclination angle α_{crit} marks the point of the change from convective to absolute Rayleigh-Taylor instability. As soon as $\alpha > \alpha_{\mathrm{crit}}$, absolute Rayleigh-Taylor instability occurs, which is shown in case b) of Figure 2. Instabilities in the flow are not longer dampened or transported away from there point of origin due to surface forces or convective impulse transport and perturbations can grow spatially (Brun et al., 2015). The absolute Rayleigh-Taylor instability is characterized by enduring liquid droplet detachment immediately after the liquid inlet (Scheid et al., 2016). Therefore, the instability is spatial fixed along flow path due to local growth of instabilities with a propagation speed of the perturbation of zero (Brun et al., 2015). Nonlinear effects like 2D and 3D waves in the flow occur due to grown perturbations until saturation (Kofman et al., 2017). These nonlinear waves develop along the flow direction (Kalliadasis et al., 2011) caused by wave formation due to convection known as Kapitza instability (Kapitza, 1948). The effect of droplet formation along a rivulet amplifies the occurring instabilities (Ledda et al., 2020, 2021). Thus, the magnitude of the absolute Rayleigh-Taylor instability is different and is described by the determination of the relative drained liquid mass flow m_{rel} which varies regarding the Reynolds number, the inclination angle α as well as the structured surface. On this account, the relative drained liquid mass flow m_{rel} is expected to be a function of the aforementioned values.

3. Methodology and materials

In the following section, the constructed measurement cell, the experimental procedures, and the employed materials are described in detail.

3.1. Measurement cell

The measurement cell is shown in Figure 3a). The setup consists of a liquid cycle and a tiltable cell with optical measurement devices. More information on the optical measurement systems is provided in Section 3.2. The main parts of the measurement cell are displayed in the simplified P&ID in Figure 3b). The liquid is pumped from the storage vessel (V-01) through a heat exchanger (HE-02) to the measurement cell. To ensure a constant feed temperature of (25.0 ± 0.1) °C (TI-01), the heat exchanger is connected to a thermostat Julabo FP-40 (HE-01). The liquid feed flow rate is monitored via a coriolis mass flow meter Sitrans FC Massflow Mass 2100 from Siemens (FIC-01) and controlled by a frequency-controlled gear pump Verder VGS096 (P-

01), while the pressure is tracked using a Optibar pressure sensor from Krohne (PI-01). The liquid is pumped through a liquid distributor, which enables a uniform distribution over the plate width. In order to gain reproducible inlet conditions at all inclination angles, the liquid distributor is designed as a mixing chamber with a internal distributor and an outlet with a 1 mm gap over a length of 220 mm. This design enables film flow conditions at the liquid inlet for all investigated inclination angles.

The measurement cell and the optical sensor equipment is mounted on the same construction frame, pivoted on ball bearings, and connected to a planetary geared stepper motor. Thus, any plate inclination can be realized. The theoretical error of the experimental inclination angle is $\pm 0.01°$. All experiments were conducted on anodized aluminum surfaces with a dimension of 220 mm in width and 500 mm in length.

The drained liquid is collected in a vessel (scale) whose mass is measured via a scale system Combics Pro equipped with Combics plattform CAPS1-60FE-NCE from Sartorius (MM-01) and recorded over time until the vessel is full. At this point, all collected liquid is returned to the storage tank (V-01) using a gear pump BVP-Z from Ismatec (P-02). The liquid that remains on the plate is conveyed to V-01 using a gear pump BVP-Z from Ismatec (P-03).

The liquid component system is composed of deionized water, Marlipal 24/70 from Sasol, and rhodamine B from Fluka. The non-ionic surfactant Marlipal was added to ensure a fully wetted surface and its concentration c was kept above 100 $\mathrm{mg\,L^{-1}}$, to ensure optimal wetting properties. The concentration is more than two times higher than the critical micellar concentration reported by Paul (2014), resulting in significant amount of surfactant

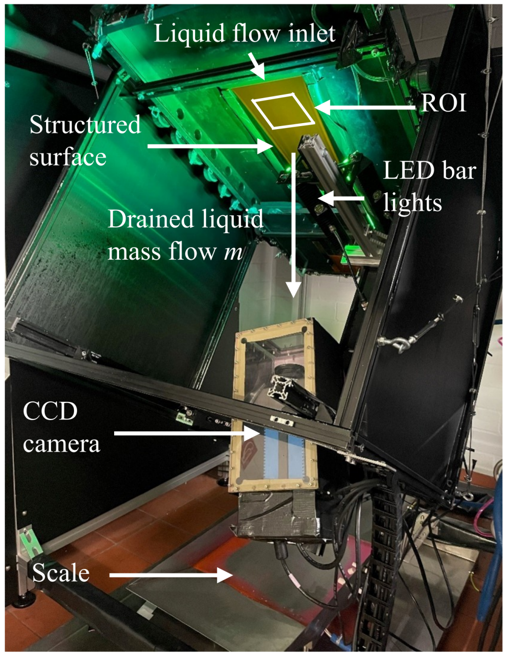

a)

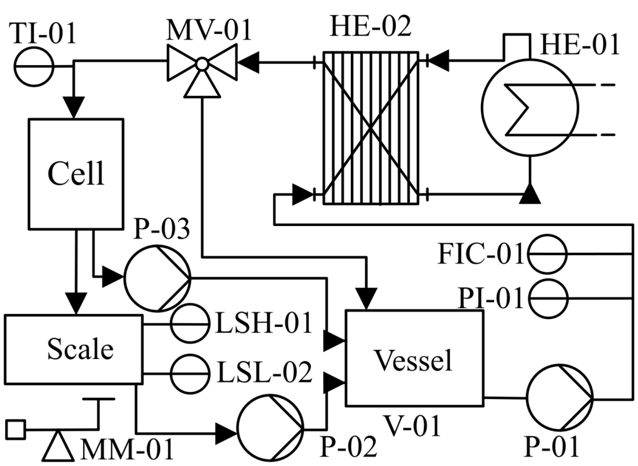

b)

Figure 3: Film flow testing rig with optical measurement technology a) schematic overview of actual facility b) simplified P&ID flowsheet of the rig.

in the bulk phase, so that the influence of Marangoni effects during droplet formation is reduced. The surfactant addition resulted in a surface tension $\sigma_\mathrm{l} \leq 0.033\,\mathrm{N\,m^{-1}}$. This was regularly verified using a Krüss tensiometer K100 equipped with the Wilhelmy plate method for a temperature of 25 °C. The kinematic viscosity for water at 25 °C was used for calculations based on (Korson et al., 1969). Simultaneously, the dynamic viscosity of the liquid, μ_l, was measured at 25 °C using the rotational viscometer Haake viscotester iQ. The liquid density ρ_l was determined using the installed coriolis sensor. Rhodamine B was added as a fluorescence tracer at a concentration around $5\,\mathrm{mg\,L^{-1}}$. Next to a pratical smooth surface, a 2D wave and a 3D pyramidal microstructured surface as shown in Figure 4 were designed to study the influence of a structured surfaces on the flow stability. The 2D wave structure is shown in Figure 4a) and the 3D pyramidal structure is shown in Figure 4b). Based on the work of Zhao and Cerro (1992), the structure height was chosen to achieve a ratio $0.1 < \delta^* < 1$ for the ratio of expected film thickness and structure height. Thus, both surfaces have an amplitude of 1 mm, because an interaction of the surface and the liquid flow is expected. The surfaces are made of aluminum treated with a black anodized coating without additional surface sealing and the texture starting directly after the liquid inlet.

3.2. Light-induced Fluorescence

In general, light-induced fluorescence (LIF) is an optical measurement technique based on the excitation of a dissolved fluorescence dye with an external laser or light source. The tracer-specific emission spectrum is detected using an optical detection device. Droplets, rivulets and thin film flows were experimentally investigated using LED-induced fluorescence (Hagemeier

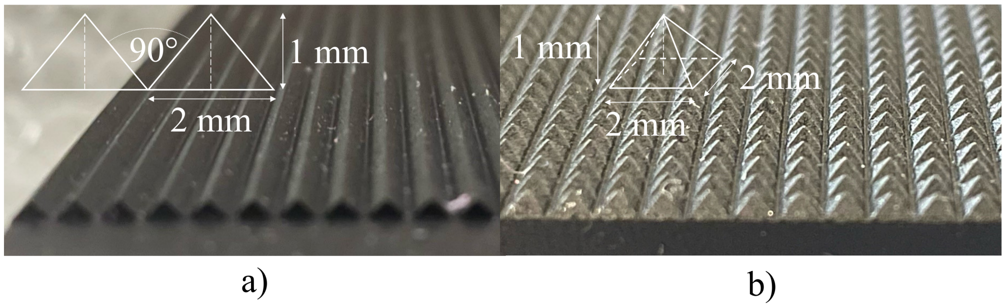

Figure 4: Geometries of the examined structured surfaces with their geometric dimensions: a) 2D wave structured surface; b) 3D pyramidal structured surface.

et al., 2012). LIF was successfully applied for film thickness measurement on structured packing materials in our previous work Leuner et al. (2018a,b).

The experimental setup contains two green-light bar LEDs LB250 from iiM AG (see Figure 3a)) with a wavelength of $\lambda_{\mathrm{ex}} = 528\,\mathrm{nm}$ to ensure constant and reproducible illumination during the measurements. Using this excitation light source, the dissolved fluorescence tracer rhodamine B is illuminated and then emits light at wavelengths λ_{em} between 550 and 650 nm. A lens with 50 mm focal length and a variable aperture was assembled on the camera (type: charged-coupled device, CCD). For pixelwise intensity detection, a pco.2000 CCD camera from Excelitas PCO GmbH was used. The camera was protected by a splash guard with optical access. To avoid spectral interference effects of the tracer, an optical red-light bandpass filter was mounted onto the lens.

3.3. Measurement procedure

Defined initial conditions are substantial for reproducible experimental results. For this reason, all experiments were started with a fully wetted surface and an initial inclination angle of 0° (for visualization, see Figure 1). Then, the relative drained liquid mass flow $m_{\mathrm{rel,exp}}$ was determined for varying inclination angles by rotating the plate. Once the liquid begins to drip from the plate, a measurement time of at least 180 s was recorded to ensure a steady state. The determination of α_{crit} is directly linked to the weighing of drained liquid, without the optical measurement technique being able to detect liquid draining positions more than 200 mm from the liquid inlet. Additionally, the velocity field of the liquid film flow was not investigated experimentally. In the experimental setup, the convective and absolute Rayleigh-Taylor instability are superimposed. Based on the previous listing of the experimental boundary conditions and the detailed discussion on the transition of absolute to convective instability in Section 2, we define the critical inclination angle as $\alpha^{*}_{\mathrm{crit,exp}}$. This angle marks the beginning of an unstable film flow with droplet detachment due to convective Rayleigh-Taylor instability in combination with a possible superimposed Kapitza instability Rietz et al. (2017). Due to the investigated region of inclination angle, absolute Rayleigh-Taylor instability definitely occurs. To experimentally investigate both effects separately, a very high resolving measurement technique would be necessary. Moreover, the application of such technique would be related to very high effort. The focus of this work was to investigate the influence of structured surfaces on film stability (i.e. droplet formation) on a larger scale. Likewise, an evaluation based on the position of liquid detachment is difficult, because "occurring already in the vicinity of the inlet" as mentioned by Scheid et al. (2016), is a relative broad definition for the experimental determination of the onset of absolute Rayleigh-Taylor instability without investigating the velocity field experimentally. The critical inclination angle $\alpha^*_{\mathrm{crit,exp}}$ is found when 1% of the liquid feed drains from the plate into the tub. Two experimental runs were performed to determine the critical inclination angle α^*_{crit} and the relative drained liquid mass flow m and the mean value of both runs is reported in the figures of Section 4. In the experiments, a flow path of 500 mm was investigated with LIF measurements covering a maximum recording area of 200 mm in length.

The measurement of the film thickness was carried out as a single determination according to a pre-defined methodology: images for background correction and illumination correction had been taken before a measurement sequence was started. The fluorescence intensity signal was calibrated using a similar wedge calibration cuvette as described by Bonart et al. (2017). The LIF measurements were carried out on a fixed region of interest with a size of $10\,\mathrm{cm}^2$ (square in the middle of the surface structure and marked in Figure 3a)). The post-processing is carried out as follows:

1. Loading of raw image data;
2. Pixel-wise calculation of mean values based on raw image data;
3. Offset calibration (due to minimal mechanical distortion) based on the actual inclination angle;
4. Setting of ROI;
5. Pixel-wise substraction of background noise from the current image with average values;

6. Pixel-wise illumination correction (less excitation light intensity leads to lower fluorescence signal);

7. Calculation of calibration curve based on measured intensity along the wedge cuvette in consideration of temperature changes during the calibration procedure (no temperature control of the cuvette);

8. Pixel-wise calculation of the film thickness based on the calibration curve;

9. Calculation of average value for film thickness for the whole ROI;

To conclude the Section 3, we investigated five different Reynolds numbers between 28.4 up to 113.5 for various inclination angles over three different surfaces. For the investigation of the critical convective inclination angle $\alpha^*_{\mathrm{crit,exp}}$ and the drained liquid mass flow $m_{\mathrm{rel,exp}}$ an inclination angle $\alpha = 0°$ was set and the critical convective angle with large angular changes was determined. Afterwards, the critical convective inclination angle was investigated with an increment of the inclination angle of 1° starting at lower inclination angles than the expected critical angle up to 90°, to be able to precisely detect the dripping onset as well as the drainage flow experimentally. Likewise, the film thickness δ was determined for inclination angles between 0° and 90° and additionally compared to the critical convective inclination angle and the drained liquid mass flow for $\alpha = 0°$, 20°, 40° and 60°.

4. Results and discussion

First, the observed critical convective inclination angles for the smooth surface are shown. Then, the measurements of the relative drained liquid mass flow and film thickness are presented. In the last step, the impact of the microstructure on the film flow stability is discussed.

4.1. Critical convective inclination angle on smooth surface

The experiments on the smooth surface were carried out for an aqueous system with a Kapitza number of 1707 to be able to compare them to the numerical results obtained by Scheid et al. (2016). In addition to the measurement procedure outlined in the previous section, this also required a minimum Reynolds number of 28.4 to always ensure a fully wetted surface for a vertical liquid falling film.

Experiments for five different Reynolds numbers were performed to identify the critical convective inclination angle $\alpha^*_{\mathrm{crit,exp,smooth}}$ on the smooth surface and to determine the influence of different Reynolds numbers on the begin of droplet detachment due to convective Rayleigh-Taylor instabilities. In Table 1, the experimentally determined critical convective inclination angles of this work, correlation-based results for $\alpha_{\mathrm{crit,calc}}$ (Equation (5) given by Scheid et al. (2016)), and the simulation results of Scheid et al. (2016) for the critical inclination angle $\alpha_{\mathrm{crit,sim}}$ on the smooth surface are reported.

The calculation of the critical inclination angle $\alpha_{\mathrm{crit,calc}}$ is carried out using the correlation Equation (5) derived by Scheid et al. (2016) under the boundary condition of an imposed flow rate on a smooth surface with no inertia and no viscous extensional stress.

$$tan(\alpha^{(0)}_{\mathrm{crit}})^4\sqrt{sin(\alpha_{\mathrm{crit}})^{(0)}} \approx 2.1086\frac{Ka^{\frac{3}{2}}}{Re} \tag{5}$$

The results for $\alpha^*_{\mathrm{crit,exp,smooth}}$ and $\alpha_{\mathrm{crit,calc}}$ show a decreasing critical inclination angle for rising Reynolds numbers. In addition to these values,

Table 1: Comparison of critical convective inclination angles $\alpha^*_{\mathrm{crit,exp}}$ with literature data (Scheid et al., 2016) for various Reynolds numbers Re and a Kapitza number ≈ 1707 on a smooth surface.

Quantity	Values				
Re	28.4	35.5	42.6	85.1	113.5
$\alpha^*_{\mathrm{crit,exp,smooth}}$ (this work)	84.4°	84.4°	82.5°	80.5°	80.5°
$\alpha_{\mathrm{crit,calc}}$ (Scheid et al., 2016)	83.3°	82.9°	82.6°	81.2°	80.6°
$\alpha_{\mathrm{crit,sim}}$ (Scheid et al., 2016)	84.4°	85.0°	85.3°	87.3°	87.9°

simulation results (read from a diagram of Scheid et al. (2016) for Kapitza number of 1000) show an increase of $\alpha_{\mathrm{crit,sim}}$ as the Reynolds number increases. Scheid et al. (2016) predicted a minimum of the critical inclination angle for a Reynolds number ≈ 8. However, we could not ensure a fully wetted surface for these operating conditions and could therefore not verify this minimum experimentally.

Overall, the simulation results show an opposite trend to our experimental results. In the simulation study of Scheid et al. (2016) the velocity field and the propagation speed of perturbations were investigated. Exclusively for Reynolds numbers 28.4 and 35.5, an agreement with the experiments could be found, which lies directly in the region of the validity of the model from Scheid et al. (2016). The stabilization effect of higher Reynolds numbers in the region of prevailing inertia (above the minimal critical angle) as reported by Scheid et al. (2016) could not be reproduced without measuring the velocity field. In contrast, the transition modeled by Scheid et al. (2016) is based on a linear transition method while omitting any experimental non-idealities as well as non-linear instability phenomena. On the other hand, the results match well with the correlation-based results in terms of trend and deviation (Scheid et al., 2016). Over the entire range of Reynolds numbers, the deviation across all measured critical convective inclination angles is below 2°. These minor deviations between the experimental results and the correlation-based data can be explained with non-idealities in comparison with the numerical results, e.g., the practical smooth surface in the experiment compared to an ideal smooth surface in the simulation. In addition, minor liquid maldistributions can lead to slightly asymmetrical flow patterns, which then result in variation of the film thickness with the width. Also, significant changes in the flow regime along the flow direction appear and rivulet confluence is observed in our experiments, which could result in earlier liquid dripping (Rietz et al., 2017). The experimental studies by Brun et al. (2015) showed a decrease of α_{crit} for an increasing ratio of initial film thickness to capillary length. The overall trend of our experimental data for $\alpha^{*}_{\mathrm{crit,exp,smooth}}$ confirm the experimental results from Brun et al. (2015).

The decreasing critical convective inclination angle observed in this work can be explained by a change in the flow pattern as the inclination angle increases. Therefore, the film tears open and parallel rivulets are formed (as will be shown in Figure 6. Convective Rayleigh-Taylor instabilities are growing along the flow direction and perturbations increase with higher Reynolds number. In consequence, both effects lead to a lower critical convective inclination angle with rising Reynolds number. For higher inclination angles, the liquid film laces up and becomes thicker. In addition, the liquid film constricts and lead for a non dripping film to a smaller flow width, which is superimposed with the increase in film thickness. Also the flow morphology changes to parallel rivulet flow and this results in a velocity field, which is not covered by the Nusselt solution. Due to these sidewall effects the cross-sectional area flowed through changes, which influences the flow velocity. Nevertheless, without measuring the velocity field a conclusive statement on the local Reynolds number cannot be made. In summary, liquid detachment is influenced by the Reynolds number, the flow pattern (i.e., film flow or rivulet flow), the effective growth of convective Rayleigh-Taylor instabilities along the flow direction within the different flow patterns, and the ratio of local liquid film thickness to capillary length as found by Brun et al. (2015).

4.2. Investigation of drained liquid flow and average film thickness on smooth surface

After the critical convective inclination angle is exceeded, liquid detaches from the flow. A quantification of the relative drained liquid mass flow $m_{\mathrm{rel,exp}}$ was carried out for five different Reynolds numbers and for inclinations between vertical and horizontal orientation of the surface. For inclination angles from 0° up to 90°, the mean liquid film thickness $\delta_{\mathrm{mean,exp,smooth}}$ was measured using LIF.

Figure 5 shows the percentage of drained liquid in relation to the liquid feed on the smooth surface, $m_{\mathrm{rel,exp,smooth}}$, as a function of the inclination angle α under variation of the Reynolds number. Inclination angles significantly lower than $\alpha^{*}_{\mathrm{crit,exp}}$ are not shown because no liquid drains off at this inclinations. In Figure 5 the relative drained liquid mass flow is shown over the inclination angle α. For a constant Reynolds number and a rising inclination angle α, the relative drained liquid mass flow $m_{\mathrm{rel,exp,smooth}}$ increases contin-

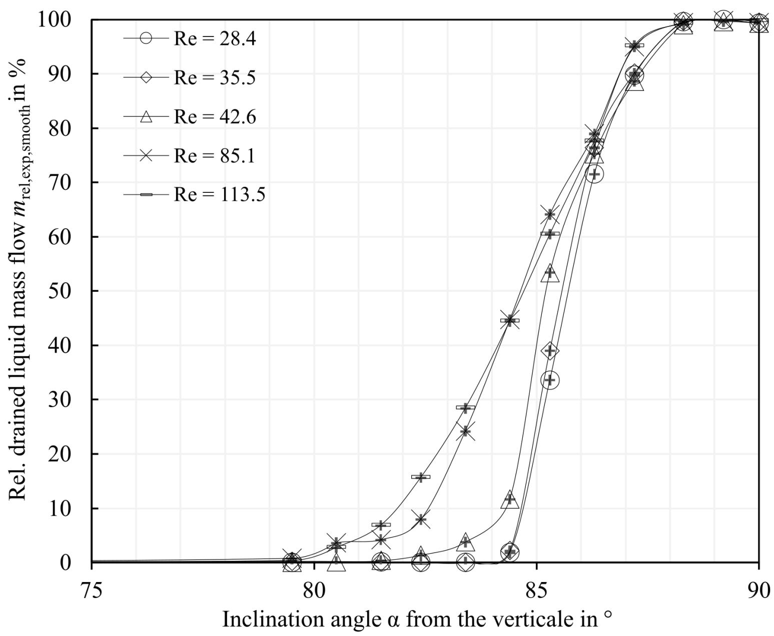

Figure 5: Relative drained liquid mass flow $m_{\text{rel,exp,smooth}}$ over the inclination angle α for a Kapitza number of 1707 and different Reynolds numbers on a smooth surface at T = 25 °C. Lines between data points added to guide the eye.

uously. For a constant inclination angle the relative drained liquid mass flow $m_{\text{rel,exp,smooth}}$ increases with increasing Reynolds number. For low Reynolds numbers, the liquid flow is not dominated by inertia forces, and the liquid drains almost completely at angles slightly above the critical convective inclination angle. For larger Reynolds numbers, drainage occurs earlier but the percentage of drained liquid rises less strongly (Figure 5). For inclination angles above 86°, the drainage behavior becomes almost independent of the Reynolds number.

From Figure 5 can also be seen, that the critical convective inclination angle $\alpha^*_{\text{crit,exp}}$ decreases with rising Reynolds number. Here, no stabilization

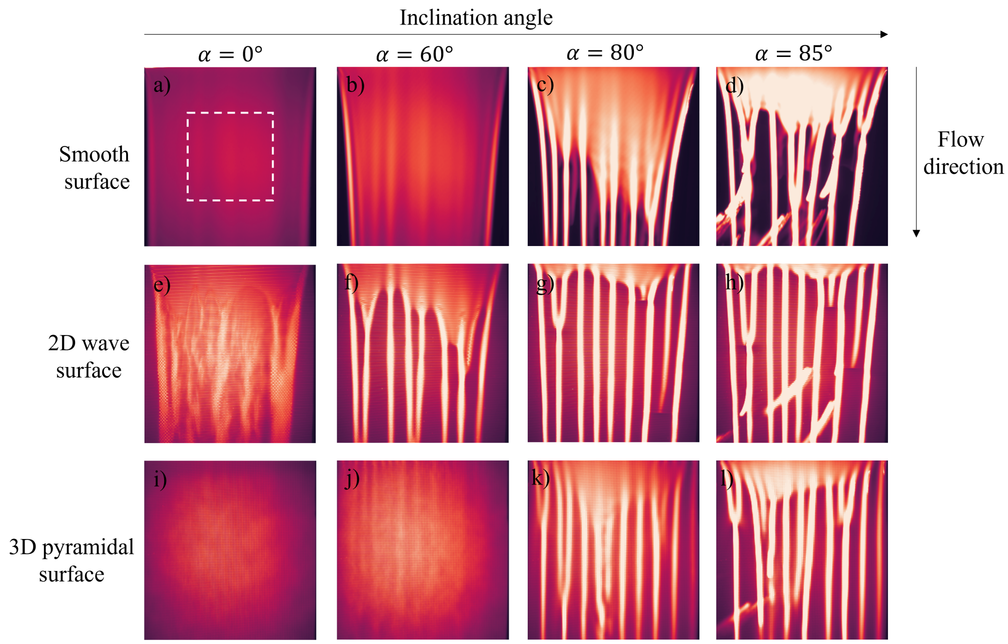

Figure 6: Liquid flow regimes on all investigated surfaces for four different values of α and for a constant Reynolds number of 113.5. In a) to d) the flow regime on a smooth surface, in e) to h) the flow regime on the 2D wave structure and in i) to l) the flow regime on the 3D pyramidal structure is presented. The white dashed square shows the ROI for the LIF measurements.

effect with higher Reynolds numbers is found, which is contrary to the simulation results reported by Scheid et al. (2016). However, Scheid et al. (2016) modeled only the linear transition between both forms of the Rayleigh-Taylor instability and liquid drainage can be influenced by non-idealities and non-linearities. In Figure 6, measured flow regimes at four different inclination angles on all investigated surfaces are depicted at Re = 113.5. For inclination angles between 0° and 60°, a film flow is observed for the smooth surface and the 3D pyramidal structure. A disturbed film flow is found for the 2D wave structure for $\alpha = 0°$, which then develops into a parallel rivulet flow for $\alpha = 60°$. For $\alpha = 80°$, the quantity of parallel rivulets generally increases, but a significant fraction of the flow remains as a film flow for the smooth and 3D surface. However, parallel rivulets remain the prevailing flow regime on the 2D structure. Once an inclination angle of 85° is set, the critical convective angle is exceeded on all surface and a region of permanent liquid detachment is reached. Therefore, a significant amount of liquid drains from the rivulets and the film flow. Over the length of the plate, it transitions into a ripped film flow and until it forms a parallel rivulet flow. In accordance with the flow regimes shown in Figure 6 a) to d), random and non-controllable rivulet confluence is observed.

In addition to the experimental results for the relative drained liquid mass flow $m_{\mathrm{rel,exp,smooth}}$ and the presented flow patterns, we have investigated the mean liquid film thickness $\delta_{\mathrm{mean,exp,smooth}}$. The film thickness was measured for the range of α from 0° to 90° at different Reynolds numbers on a smooth surface and is shown in Figure 7. The results for the vertical falling film are given in Table 2 and are compared with the theoretical values obtained from the Nusselt correlation Equation (2). A good agreement between the values calculated with Equation (2) and our experimental data using light-induced fluorescence was determined, including the expected increase of the film thickness with increasing Reynolds number (Table 2). A mean film thickness of 0.181 mm and a mean film thickness of 0.294 mm for the lowest (28.4) and largest Reynolds number (113.5) is shown in Table 2. Due to the good agreement of the measured film thickness with the theoretical Nusselt solution, we deem the LIF method suitable to measure the film thickness at

Table 2: Mean liquid film thickness calculated with Nusselts solution and measured for the case of a vertical falling film $\alpha = 0°$ at T = 25°C and a Kapitza number = 1707.

Quantity	Values				
Re	28.4	35.5	42.6	85.1	113.5
$\delta_{\mathrm{mean,exp,smooth}}$ in mm (this work)	0.181	0.199	0.211	0.280	0.294
δ_{mean} in mm (Equation (2))	0.190	0.205	0.218	0.274	0.302

other inclination angles.

From Figure 7 it can be seen, that the film thickness increases moderately while $\alpha \leq 60°$, which is caused by the stronger inclination of the plate and the resulting reduced acceleration in the imposed flow direction (Leuner et al., 2018b). When the inclination is increased beyond 79°, the behavior of the film thickness depends highly on the Reynolds number: for the larger Reynolds numbers (85.1 and 113.5), the film thickness hardly changes but then increases almost exponentially up to 87°. For the smaller Reynolds numbers (28.4 to 42.6), the film thickness remains almost constant for angles up to 85°. The larger inclination angles also cause a significant amount of relative drained liquid mass flow $m_{\mathrm{rel,exp,smooth}}$. Because dripping occurs after longer flow length indicating a convective Rayleigh-Taylor instability, the film thickness measurement is not affected. Thus, the liquid film thickness $\delta_{\mathrm{mean,exp,smooth}}$ shows a slight increase due to the chosen ROI of the LIF measurements: for α between 85° and 87°, droplet detachment from both the closed liquid film and the rivulets occurs. This drainage behavior out of the rivulet flow pattern was also found by Ledda et al. (2020, 2021). The appearance of droplets increases the measurement error of LIF method because

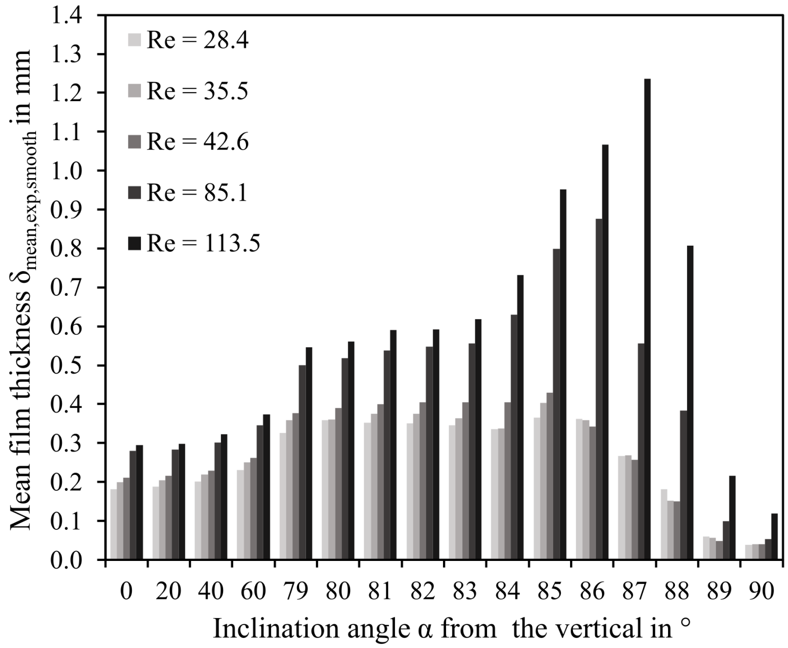

Figure 7: Mean liquid film thickness $\delta_{\mathrm{mean,exp,smooth}}$ over the inclination angle α for Kapitza number = 1707 on a smooth surface for different Reynolds numbers at T = 25 °C (angles rounded to integer values).

the more intensively illuminated droplets changes the results for the measure film thickness. For inclination angles above 85° (small Reynolds numbers) and 87° (high Reynolds numbers), respectively, a significant decrease of the film thickness is found. For Reynolds numbers between 28.4 up to 42.6 the percentage decrease for the film thickness per degree is about 10 %, about 26 % for Re = 85.1 and about 37 % for Re = 113.5. The measured film thickness for α between 89° and 90° is caused by still adhering liquid. Shortly after the liquid inlet, all liquid drips off the surface completely. An increased measurement time before taking the images would lead to $\delta_{\mathrm{mean,exp,smooth}} \approx 0$ for each Reynolds number due to the slow drying of the surface.

A destabilization effect of higher Reynolds numbers was found for the critical convective inclination angle $\alpha^*_{\text{crit,exp,smooth}}$ and the relative drained liquid mass flow $m_{\text{rel,exp,smooth}}$. This can be attributed to the increase of the mean film thickness $\delta_{\text{mean,exp,smooth}}$, which results in a rising ratio of film thickness to constant capillary length (Brun et al., 2015), resulting in lower critical convective inclination angle. These effects cause droplet formation on top of the film, e.g., in the form of rivulets (Fermigier et al., 1992), and shifts the critical convective inclination angle for higher Reynolds numbers to lower values. The higher local film thickness in the region of observed parallel rivulets shown in Figure 6a) to d), seems to exceed the ratio of film thickness to capillary length found by Brun et al. (2015) and no counteracting effect of flow stabilization due to higher liquid loads is found.

4.3. Investigation of critical convective inclination angle, drained liquid flow, and average film thickness on structured surfaces

The influence of the structured surface on the fluid dynamics of gravity-destabilized liquid is of major importance as it may stabilize or further destabilize the flow.

As shown in Table 3, $\alpha^*_{\text{crit,exp}}$ generally decreases with increasing Reynolds number across all investigated structured surfaces. However, a divergence from this general trend is found for Re = 35.5 and Re = 42.6 on the 2D wave structure. The deviation from the general trend found could be explained by the fact that for very small Reynolds numbers (28.4) the flow is strongly slowed down resulting in liquid detachment. For larger Reynolds numbers (85.1 and 113.5), perturbations increase more and convective Rayleigh-Taylor instability is highly promoted. The other two lie between both conditions, so that the onset occurs later due to more favorable flow conditions. However, we found higher $\alpha^*_{\text{crit,exp}}$ for the Reynolds numbers (35.5 and 42.6) the general trend of the dripping behavior is similiar as shown in Figure 8.

Table 3: Comparison of the critical convective inclination angle for the smooth place, a 2D wave structure (Kapitza number = 1761), and a 3D pyramidal structure (Kapitza number = 1703) at various Reynolds numbers for T = 25 °C.

Quantity	Values				
Re	28.4	35.5	42.6	85.1	113.5
$\alpha^*_{\text{crit,exp,smooth}}$	84.4°	84.4°	82.5°	80.5°	80.5°
$\alpha^*_{\text{crit,exp,2D}}$	81.0°	83.0°	84.0°	75.0°	69.0°
$\alpha^*_{\text{crit,exp.,3D}}$	86.0°	85.0°	85.0°	82.0°	83.0°

Beside the investigation of $\alpha^*_{\text{crit,exp}}$, the relative drained liquid mass flow $m_{\text{rel,exp}}$ for different structured surfaces and different Reynolds numbers was investigated as shown in Figure 8. In Figure 8a), the drained liquid mass flow $m_{\text{rel,exp,2D}}$ is shown for varying Reynolds number over the inclination angle α for the 2D wave structure. Just as with the smooth surface, $m_{\text{rel,exp,2D}}$ also increases. However, an earlier liquid detachment and a broader range of α are observed. Most importantly, an increase of the Reynolds number causes a noticeably higher relative drained liquid mass flow $m_{\text{rel,exp,2D}}$. Hence, a negative influence of the 2D wave structure on the stability of the liquid flow is found compared to the smooth surface in Figure 5. In terms of flow regimes, we observed both a filled 2D wave structure and a overflow of the liquid (Figure 6 e) to h)). As the inclination angle increases, a ripped film flow and parallel rivulets evolve sooner than on the smooth surface. The 2D waves

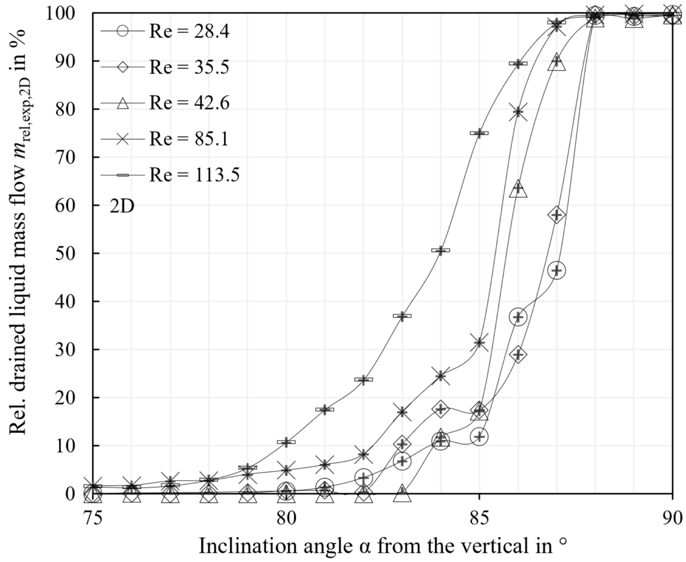

a)

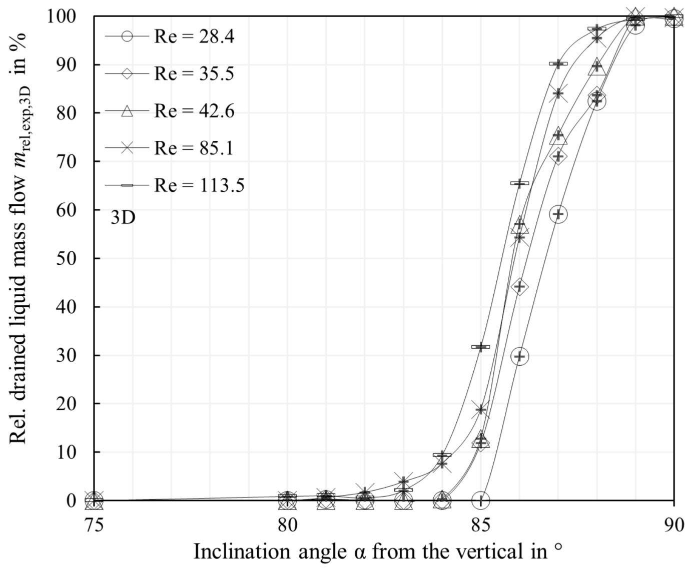

b)

Figure 8: Relative drained liquid mass flow over the inclination angle α at T = 25 °C for different Reynolds numbers a) $m_{\mathrm{rel,exp,2D}}$ on a 2D wave structured surface for Kapitza number = 1761 and b) $m_{\mathrm{rel,exp,3D}}$ for Kapitza number = 1703 on a 3D pyramidal structure. Lines between data points added to guide the eye.

orthogonal to the liquid flow direction lead to stronger flow perturbations due to the structure, which results in increased Rayleigh-Taylor instability. These perturbations accumulate much faster along the flow direction compared to the smooth surface and in the most cases dripping occurs at smaller angles.

For the investigated 3D pyramidal structure, the liquid can flow through the channels between the pyramids along the convective flow direction. This flow path between the structures prevents overflow of the structures. Consequently, the liquid distribution is better and and fewer perturbations due to the structured surface occur. In Figure 8b), the drained liquid mass flow $m_{\mathrm{rel,exp,3D}}$ is plotted over the inclination angle α for varied Reynolds numbers for the 3D pyramidal structure. Liquid detachment occurs for a narrow range of the inclination angle α and the resulting relative drained liquid mass flow $m_{\mathrm{rel,exp,3D}}$ depends less on the Reynolds number. Due to the lower dependence of the critical convective inclination angle and the relative drained liquid mass flow on the Reynolds number, perturbations caused by the convective flow seem to be reduced or damped. This indicates a stabilization effect on the gravity-destabilized film flow for 3D pyramidal structures. Due to the more homogeneous liquid distribution caused by the 3D structure, the local film thickness distribution is more uniform and local maxima seem to be reduced. Thus the ratio between film thickness to capillary length by Brun et al. (2015) is exceeded only for larger inclination angles, when the film thickness increases significantly due to the reduced convection and thus lower liquid velocities.

In Figure 9a), the mean liquid film thickness $\delta_{\mathrm{mean,exp,2D}}$ for varying Reynolds number over increasing α is shown. At constant Reynolds number,

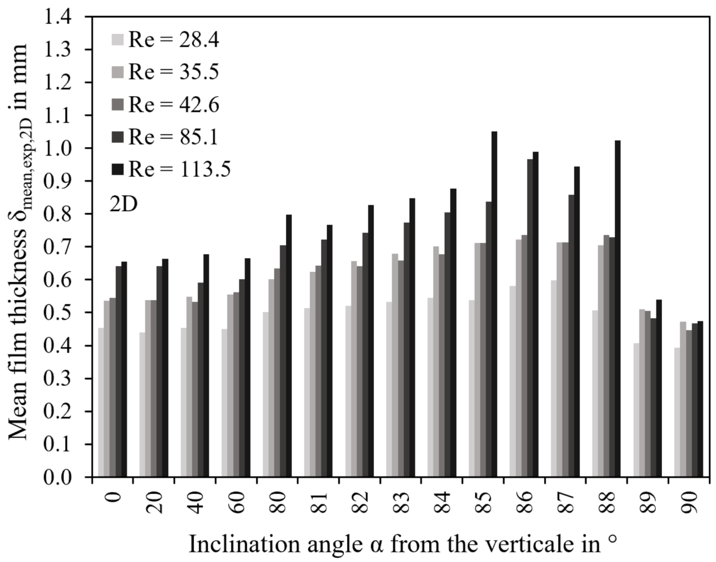

a)

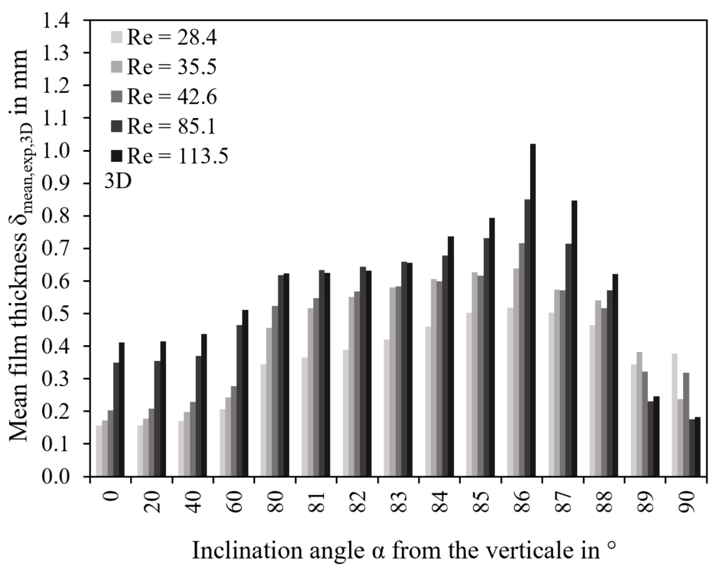

b)

Figure 9: Mean liquid film thickness $\delta_{\mathrm{mean,exp}}$ for different Reynolds numbers: a) for Kapitza number = 1761 on a 2D wave structured surface; b) for a Kapitza number = 1703 on a 3D pyramidal structure.

the mean film thickness $\delta_{\text{mean,exp,2D}}$ remains almost the same for inclination angles between 0° and 60°. This constant film thickness is caused by the valleys in the wave structure that are always filled with liquid. In addition to the increasing mean film thickness with higher Reynolds numbers, more waves are observed, which are caused by the sharp edges of the orthogonal 2D edges. Overall, an increase of the mean film thickness $\delta_{\text{mean,exp,2D}}$ compared to the smooth surface Figure 7 is found.

In the range of α from 80° to 84°, only a minor increase of δ is detected. For even larger inclination angles, a certain amount of liquid remains in the valleys of the structure for all Reynolds numbers, which justifies the assumption of a constant static liquid holdup. In conclusion, the 2D wave structure seems to have a negative influence on the film stability and seems to enhance convective Rayleigh-Taylor instabilities.

In Figure 9b), the measured mean liquid film thickness for varying Reynolds number for increasing inclination angle α over the 3D pyramidal structure is shown. For inclination angles in the range of 0° to 60°, only a slight increase of the mean film thickness is observed. This trend is comparable to the smooth surface shown in Figure 7.

The mean film thickness $\delta_{\text{mean,exp,3D}}$ at different Reynolds numbers and inclination angles turns out to be larger compared to the smooth surface and lower compared to the 2D wave structure. Nonetheless, a lower liquid film thickness for Reynolds numbers from 28.4 to 42.6 is found and could be caused by liquid acceleration through the cross-section between the pyramidal structure along the flow pathway.

For α in the range from 80° to 84°, the largest increase of δ is observed for Re = 28.4. This indicates a high influence of the structure on the liquid flow. Thus, a strong increase in the liquid holdup within the structure is conceivable and indicates a partially filled structured surface. Additionally, the lower increase of the film thickness with rising Reynolds number compared to the smooth surface indicates a larger liquid holdup with a plateau starting at Re > 85.1.

Due to the improved liquid distribution caused by the 3D pyramidal structure, a more uniformly film flow compared to the smooth and 2D wave surface is observed (Figure 6i) to l)).

In comparison with the smooth surface and the 2D wave structure, a larger $\alpha^*_{\mathrm{crit,exp,3D}}$ on the 3D pyramidal structure could be found for the investigated Reynolds numbers. Additionally, the narrower range of the inclination angle α over the whole range of Reynolds numbers for the relative drained liquid mass flow $m_{\mathrm{rel,exp,3D}}$ indicates a stabilization effect of the 3D pyramidal structure on the film flow. Given the improved liquid distribution across the whole surface due to improved cross mixing, the 3D structure seems to stabilize the film flow and suppresses Rayleigh-Taylor instabilities.

5. Conclusion and Outlook

In this contribution, a measurement cell for the investigation of gravity-destabilized film flows, i.e., film flows with negative inclination angles was introduced and applied. It is aimed at closing the gap in experimentally characterizing and understanding such flow regimes, which is present up till now.

Experimental results for the critical convective inclination angle $\alpha^*_{\mathrm{crit,exp}}$, the relative drained liquid mass flow $m_{\mathrm{rel,exp}}$, and the mean liquid film thickness $\delta_{\mathrm{mean,exp}}$ for a smooth, a 2D wave, and a 3D pyramidal structured solid surface were presented the first time. We compared our experimental results at Reynolds numbers between 28.4 up to 113.5, a Kapitza number of around 1707, and a smooth surface to literature data by Scheid et al. (2016). This comparison showed good agreement. A decreasing critical convective inclination angle with rising Reynolds number was observed experimentally.

The influence of geometry was incorporated using a 2D wave structure and a 3D pyramidal structure, which were intended to represent real packing geometries. A negative influence of the 2D wave structure on the film flow stability and a stabilizing effect of the 3D pyramidal structure regarding the critical convective inclination angle, which represents the beginning of droplet detachment from the flow, was found. Mainly a decrease of the critical convective inclination angle with increasing Reynolds number could also be observed for the 2D wave structure and 3D pyramidal structure.

Furthermore, the relative drained liquid mass flow for angles above the critical convective inclination angle was quantified. A stabilizing effect of the 3D structure could be found. The relative drained mass flow was shown to be almost completely independent of the Reynolds number. In contrast, the relative drained mass flow for the smooth surface and the 2D wave structure was highly influenced by the Reynolds number.

Regarding the mean film thickness, the 2D structure showed larger values compared to the smooth and the 3D surface. Overall, a stabilizing effect on the liquid flow was discovered for the 3D pyramidal structure due to the more homogeneous film thickness.

The experimental investigations show a significant impact of the structured surfaces on the stability of gravity-destabilized film flows. These fundamental experimental results can be used to better understand the fluid dynamics within packing structures used in distillation and absorption processes. In future work, more viscous liquids should be investigated to study the influence of fluid properties on the critical convective angle and draining behavior. To this end, Kapitza numbers in the range from 0.1 to 200 are of interest. To carry out further experimental investigations and to make comparability between the results possible, the height of the structured surfaces has to be designed on the ratio δ^* in the range of 0.1 to 1 regarding the expected film thickness for higher viscous liquids.

Acknowledgements

Gefördert durch die Deutsche Forschungsgemeinschaft (DFG) - 426726119 / funded by the Deutsche Forschungsgemeinschaft (DFG, German Research Foundation) – 426726119.

References

Abdelall, F.F., Abdel-Khalik, S.I., Sadowski, D.L., Shin, S., Yoda, M., 2006. On the rayleigh–taylor instability for confined liquid films with injection through the bounding surfaces. International journal of heat and mass transfer 49, 1529–1546. doi:10.1016/j.ijheatmasstransfer.2005.07.055.

Aferka, S., Viva, A., Brunazzi, E., Marchot, P., Crine, M., Toye, D., 2011. Tomographic measurement of liquid hold up and effective interfacial area distributions in a column packed with high performance structured packings. Chemical Engineering Science 66, 3413–3422. doi:10.1016/j.ces.2011.01.022.

Al-Sibai, F., 2004. Experimentelle Untersuchung der Strömungscharakteristik und des Wärmeübergangs bei welligen Rieselfilmen. Dissertation. Rheinisch-Westfälische Technische Hochschule Aachen. Aachen, Deutschland. URL: https://publications.rwth-aachen.de/record/59863/files/59863.pdf.

Alekseenko, S., Antipin, V.A., Bobylev, A.V., Markovich, D.M., 2007. Application of piv to velocity measurements in a liquid film flowing down an inclined cylinder. Experiments in Fluids 43, 197–207. doi:10.1007/s00348-007-0322-2.

Alekseenko, S., Nakoryakov, V.E., Pokusaev, B.G., 1994. Wave flow of liquid films. begell house.

Argyriadi, K., Vlachogiannis, M., Bontozoglou, V., 2006. Experimental study of inclined film flow along periodic corrugations: The effect of wall steepness. Physics of Fluids 18, 012102. doi:10.1063/1.2163810.

Aroonwilas, A., 2001. Effects of operating and design parameters on CO2 absorption in columns with structured packings. Separation and Purification Technology 24, 403–411. doi:10.1016/S1383-5866(01)00140-X.

Billingham, J.F., Lockett, M.J., 1999. Development of a New Generation of Structured Packings for Distillation. Chemical Engineering Research and Design 77, 583–587. doi:10.1205/026387699526610.

Bonart, H., Marek, A., Repke, J.U., 2017. Experimental characterization of stable liquid rivulets on inclined surfaces: Influence of surface tension, viscosity and inclination angle on the interfacial area. Chemical Engineering Research and Design 125, 226–232. doi:10.1016/j.cherd.2017.07.022.

Bonart, H., Repke, J.U., 2018. Direct Numerical Simulations of Liquids on Microstructured Surfaces: Analysing the Fluid Dynamics on Packing. Chemical Engineering Transactions 69, 61–66. doi:10.3303/CET1869011.

Bontozoglou, V., Papapolymerou, G., 1997. Laminar film flow down a wavy incline. International journal of multiphase flow 23, 69–79. doi:10.1016/S0301-9322(96)00053-5.

Brauer, H., 1956. VDI-Forschungsheft 457. Forschung auf dem Gebiete des Ingenieurwesens .

Brauer, H., 1971. Grundlagen der Einphasen-und Mehrphasenströmungen. volume 2. Sauerländer, Aarau und Frankfurt am Main.

Brun, P.T., Damiano, A., Rieu, P., Balestra, G., Gallaire, F., 2015. Rayleigh-taylor instability under an inclined plane. Physics of Fluids 27, 084107. doi:10.1063/1.4927857.

Chandrasekhar, S., 1961. Hydrodynamic and Hydromagnetic Stability. Dover Books on Physics Series, Dover Publications, New York.

Charogiannis, A., Denner, F., van Wachem, B.G.M., Kalliadasis, S., Scheid, B., Markides, C.N., 2018. Experimental investigations of liquid falling films flowing under an inclined planar substrate. Phys. Rev. Fluids 3, 114002. URL: https://link.aps.org/doi/10.1103/PhysRevFluids.3.114002, doi:10.1103/PhysRevFluids.3.114002.

Davies, J.T., 1972. Turbulence phenomena at free surfaces. AIChE Journal 18, 169–173. doi:10.1002/aic.690180131.

Fermigier, M., Limat, L., Wesfreid, J.E., Boudinet, P., Quilliet, C., 1992. Two-dimensional patterns in Rayleigh-Taylor instability of a thin layer. Journal of Fluid Mechanics 236, 349–383. doi:10.1017/S0022112092001447.

Flagiello, D., Parisi, A., Lancia, A., Carotenuto, C., Erto, A., Di Natale, F., 2019. Seawater desulphurization scrubbing in spray and packed columns for a 4.35 mw marine diesel engine. Chemical Engineering Research and Design 148, 56–67. doi:10.1016/j.cherd.2019.05.057.

Gerke, S.J., Leuner, H., Repke, J.U., 2018. Experimental investigation of local film thickness and velocity distribution inside falling liquid films on corrugated structured packings, in: Chemical Engineering Transactions, AIDIC Servizi S.r.l.. pp. 1–6. doi:10.3303/CET1869001.

Green, C.W., Farone, J., Briley, J.K., Eldridge, R.B., Ketcham, R.A., Nightingale, B., 2007. Novel application of x-ray computed tomography: Determination of gas/liquid contact area and liquid holdup in structured packing. Industrial & Engineering Chemistry Research 46, 5734–5753. doi:10.1021/ie0701827.

Hagemeier, T., Hartmann, M., Kühle, M., Thévenin, D., Zähringer, K., 2012. Experimental characterization of thin films, droplets and rivulets using LED fluorescence. Experiments in Fluids 52, 361–374. doi:10.1007/s00348-011-1232-x.

Ishigai, S., Nakanisi, S., Koizumi, T., Oyabu, Z., 1972. Hydrodynamics and Heat Transfer of Vertical Falling Liquid Films : Part 1, Classification of Flow Regimes. Bulletin of JSME 15, 594–602. doi:10.1299/jsme1958.15.594.

Janzen, A., Steube, J., Aferka, S., Kenig, E.Y., Crine, M., Marchot, P., Toye, D., 2013. Investigation of liquid flow morphology inside a structured packing using X-ray tomography. Chemical Engineering Science 102, 451–460. doi:10.1016/j.ces.2013.08.035.

Kalliadasis, S., Ruyer-Quil, C., Scheid, B., Velarde, M.G., 2011. Falling liquid films. volume 176. Springer Science & Business Media.

Kapitza, P., 1948. Wave flow of thin viscous liquid film. Zh. Exper. Teor. Fiz. 18, 3–28.

Kapitza, P.L., Kapitza, S.P., 1949. Wave flow of thin layers of viscous liquids. part iii. experimental research of a wave flow regime. Zhurnal Eksperimentalnoi i Teoreticheskoi Fiziki 19, 105–120.

Kiss, A.A., 2019. Novel Catalytic Reactive Distillation Processes for a Sustainable Chemical Industry. Topics in Catalysis 62, 1132–1148. doi:10.1007/s11244-018-1052-9.

Kofman, N., Mergui, S., Ruyer-Quil, C., 2017. Characteristics of solitary waves on a falling liquid film sheared by a turbulent counter-current gas flow. International journal of multiphase flow 95, 22–34. doi:10.1016/j.ijmultiphaseflow.2017.05.007.

Korson, L., Drost-Hansen, W., Millero, F.J., 1969. Viscosity of water at various temperatures. The Journal of Physical Chemistry 73, 34–39. doi:10.1021/j100721a006.

Ledda, P.G., Lerisson, G., Balestra, G., Gallaire, F., 2020. Instability of a thin viscous film flowing under an inclined substrate: the emergence and stability of rivulets. Journal of Fluid Mechanics 904. doi:10.1017/jfm.2020.673.

Ledda, P.G., Lerisson, G., Balestra, G., Gallaire, F., 2021. Instability of a thin viscous film flowing under an inclined substrate: the emergence and stability of rivulets – CORRIGENDUM. Journal of Fluid Mechanics 926. doi:10.1017/jfm.2021.699.

Lel, V.V., Al-Sibai, F., Leefken, A., Renz, U., 2005. Local thickness and wave velocity measurement of wavy films with a chromatic confocal imaging method and a fluorescence intensity technique. Experiments in Fluids 39, 856–864. doi:10.1007/s00348-005-0020-x.

Lerisson, G., Ledda, P.G., Balestra, G., Gallaire, F., 2020. Instability of a thin viscous film flowing under an inclined substrate: steady patterns. Journal of Fluid Mechanics 898. doi:10.1017/jfm.2020.396.

Leuner, H., Hapke, M., Sacher, J., Grünewald, M., Repke, J.U., 2018a. An Advanced Approach to Design Structured Packing Columns using Miniaturized Experimental Set-Ups. Chemical Engineering Transactions 69, 781–786. doi:10.3303/CET1869131.

Leuner, H., Hapke, M., Sacher, J., Grünewald, M., Repke, J.U., 2018b. Miniaturized Experimental Setups as a Fundamental Element of a Promising Design Approach for Structured–Packing Columns. Chemie Ingenieur Technik doi:10.1002/cite.201800057.

Nusselt, W., 1916. Die Oberflächenkondensation des Wasserdampfes. Zeitschrift des Vereins deutscher Ingenieure 60, 1645–1648.

Paschke, S., 2011. Experimentelle Analyse ein-und zweiphasiger Filmströmungen auf glatten und strukturierten Oberflächen. Ph.D. thesis. Technische Universität Berlin. URL: https://doi.org/10.14279/depositonce-3069.

Paul, N., 2014. Theoretische und experimentelle Untersuchungen von Transport- und Grenzflächenphänomenen in mizellaren Flüssig/flüssig-Systemen. Dissertation. Technische Universität Berlin. Berlin. URL: https://api-depositonce.tu-berlin.de/server/api/core/bitstreams/3b441680-005f-4c3c-98a6-87f58870f8f9/content.

Repke, J.U., Kohrt, M., Wozny, G., 2011. Untersuchungen mehrphasiger Strömungen an einfachen geneigten Platten als potenzielles Auslegungswerkzeug für technische Trennapparate. Chemie Ingenieur Technik 83, 1107–1114. doi:10.1002/cite.201100048.

Rietz, M., Kneer, R., Scheid, B., Rohlfs, W., 2021. Spanwise structuring and rivulet formation in suspended falling liquid films. Physical Review Fluids 6. doi:10.1103/PhysRevFluids.6.084805.

Rietz, M., Scheid, B., Gallaire, F., Kofman, N., Kneer, R., Rohlfs, W., 2017. Dynamics of falling films on the outside of a vertical rotating cylinder: waves, rivulets and dripping transitions. Journal of Fluid Mechanics 832, 189–211. doi:10.1017/jfm.2017.657.

Rohlfs, W., Pischke, P., Scheid, B., 2017. Hydrodynamic waves in films flowing under an inclined plane. Physical Review Fluids 2. doi:10.1103/PhysRevFluids.2.044003.

Rohlfs, W., Scheid, B., 2015. Phase diagram for the onset of circulating waves and flow reversal in inclined falling films. Journal of Fluid Mechanics 763, 322–351. doi:10.1017/jfm.2014.684.

Scheid, B., Kofman, N., Rohlfs, W., 2016. Critical inclination for absolute/convective instability transition in inverted falling films. Physics of Fluids 28, 044107. doi:10.1063/1.4946827.

Sharp, D.H., 1984. An overview of rayleigh-taylor instability. Physica D: Nonlinear Phenomena 12, 3–18.

Shetty, S., Cerro, R.L., 1993. Flow of a thin fiom over a periodic surface. International journal of multiphase flow 19, 1013–1027. doi:10.1016/0301-9322(93)90075-6.

Spiegel, L., Duss, M., 2014. Structured Packings, in: Distillation. Elsevier, pp. 145–181. doi:10.1016/B978-0-12-386878-7.00004-8.

Szulczewska, B., Zbicinski, I., Górak, A., 2003. Liquid Flow on Structured Packing: CFD Simulation and Experimental Study. Chemical Engineering & Technology 26, 580–584. doi:10.1002/ceat.200390089.

Trifonov, Y., 2011. Counter-current gas−liquid flow between vertical corrugated plates. Chemical Engineering Science 66, 4851–4866. doi:10.1016/j.ces.2011.06.044.

Vlachogiannis, M., Bontozoglou, V., 2002. Experiments on laminar film flow along a periodic wall. Journal of Fluid Mechanics 457, 133–156. doi:10.1017/S0022112001007637.

Zhao, L., Cerro, R.L., 1992. Experimental characterization of viscous film flows over complex surfaces. International journal of multiphase flow 18, 495–516. doi:10.1016/0301-9322(92)90048-L.